Spherical Wavelets with an application in preferred crystallographic orientation

Helmut Schaeben(*), Daniel Potts(**)*, and Jürgen Prestin(**)*

(*)Mathematics and Computer Sciences in Geology
Freiberg University of Mining and Technology, Germany,

(**)Institute of Mathematics, Medical University at Lübeck, Germany

IAMG'2001, Cancun, Sep 6-12, 2001

Abstract

Several useful representations of a function $f : \Omega_p \mapsto I\!R$ exist which are usually related to specific purposes: (i) series expansion into spherical harmonics to do mathematics, (ii) series expansion into (unimodal) radial basis functions to do probability and statistics, (iii) series expansion into spline functions to do numerics. In many practical applications the common problem is to reconstruct an approximation of f from sampled data $(\mathbf{r}_i, f(\mathbf{r}_i)), i = 1, \ldots, n$, with some convenient properties using one of the above representations. Their critical parameter, e.g. (i) the degree of the harmonic series expansion, (ii) the spherical dispersion of unimodal radial functions, (iii) the choice of the knots, may to some extent be adjusted to the total number and/or the geometric arrangement of the measurement locations. However, these representations are in no way involved in the sampling process itself.

After briefly reviewing the basics of wavelets and the specifics of spherical wavelets, another representation of f in terms of spherical wavelets is introduced. It will be shown that spherical wavelets are well suited to render functions defined on a sphere. Moreover, it will be demonstrated that wavelets are well apt to allow for locally varying spatial resolution, thus providing a digital device to zoom into those spherical areas where the function f is of special interest. Such a device seems to be required to increase the spatial resolution by a factor of 1000 or greater locally. Thus, spherical wavelets provide the means to control the sampling process to gradually adapt automatically to a local refinement of the spatial resolution. In particular, it is shown that spherical wavelets apply to X–ray pole intensity data as well as to crystallographic orientation density functions, and that the multiscale resolution easily transfers from pole spheres to orientation space.

KEYWORDS: spherical wavelets, spherical multiscale representation, spherical multiresolution analysis

*Research supported in part by the EU Research Training Network MINGLE, RTN1-1999-00212

Introduction

A polynomial $H_n(x_1, \ldots, x_p)$ is homogeneous of degree n in p variables $x_1, \ldots, x_p$ if

$$H_n(tx_1, \ldots, tx_p) = t^n H_n(x_1, \ldots, x_p) \, .$$

With the Laplace operator in p dimensions

$$\Delta_p F = \sum_{i=1}^{p} \frac{\partial^2 F}{\partial {x_i}^2}$$

where x_i, $i = 1, \ldots, p$, denote Cartesian coordinates in $I\!R^p$, any polynomial $R_n(x_1, \ldots, x_p)$ satisfying

$$\Delta_p R_n = 0$$

is said to be a harmonic polynomial. The total number of linearly independent, homogeneous harmonic polynomials of degree n in p variables is

$$N(p,n) = \frac{2n+p-2}{n} \binom{n+p-3}{n-1} \, ,$$

e.g. $N(2,n) = 2$, $N(3,n) = 2n+1$, $N(4,n) = (n+1)^2$.

A homogeneous harmonic polynomial H_n of degree n in p variables may be written as

$$H_n(\mathbf{x}) = H_n(\|\mathbf{x}\| \frac{\mathbf{x}}{\|\mathbf{x}\|}) = r^n Y_n(\mathbf{r})$$

and Y_n is referred to as spherical harmonic in p dimensions, (cf. Hochstadt, 1986).

Let $\Omega_p = \{\mathbf{x} \in I\!R^p \mid \|\mathbf{x}\| = 1\}$ denote the unit sphere in p dimensions, and $d\omega_p$ its surface element such that

$$\omega_p = \int_{\Omega_p} d\omega_p = \frac{2\pi^{p/2}}{\Gamma(p/2)} \, ,$$

e.g. $\omega_2 = 2\pi$, $\omega_3 = 4\pi$, $\omega_4 = 2\pi^2$.

Any two spherical harmonics of different degree are orthogonal on the sphere, i.e.

$$\int_{\Omega_p} Y_n(\mathbf{r}) Y_k(\mathbf{r}) d\omega_p = 0$$

for $n \neq k$. If $\{Y_n\}$ is a set of $N(p,n)$ linearly independent spherical harmonics, then it is possible to construct an orthonormal set $Y_{n,1}, \ldots Y_{n,N(p,n)}$, i.e.

$$\int_{\Omega_p} Y_{n,j}(\mathbf{r}) Y_{n,k}(\mathbf{r}) d\omega_p = \delta_{j,k}$$

It can be shown that

$$\sum_{j=1}^{N(p,n)} Y_{n,j}(\mathbf{r}_1) Y_{n,j}(\mathbf{r}_2) = \frac{N(p,n)}{\omega_p} P_n(\mathbf{r}_1 \cdot \mathbf{r}_2)$$

where P_n are the Legendre polynomials of degree n in p dimensions.

Furthermore, every spherical harmonic can be represented as a linear combination of Legendre polynomials in the form

$$Y_n(\mathbf{r}) = \sum_{j=1}^{N(p,n)} c_j P_n(\mathbf{r}\cdot\mathbf{r}_j)$$

for a suitably chosen set of unit vectors $\mathbf{r}_j \in \Omega_p$, $j = 1, \ldots, N(p,n)$. The Legendre polynomials provide the reproducing kernel, i.e.

$$Y_n(\mathbf{r}) = \frac{N(p,n)}{\omega_p} \int_{\Omega_p} Y_n(\mathbf{r}')P_n(\mathbf{r}\cdot\mathbf{r}')\, .d\omega_p$$

Eventually, it should be noted that the Legendre polynomials in p dimensions are essentially the Gegenbauer polynomials

$$C_n^{(p+2)/2}(t) = \binom{n+p-3}{n} P_n(t)\,.$$

The Funk-Hecke theorem states that

$$\int_{\Omega_p} f(\mathbf{r}_1\cdot\mathbf{r}_2)Y_n(\mathbf{r}_2)d\omega_p = \omega_{p-1}Y_n(\mathbf{r}_1)\int_{-1}^{1} f(t)P_n(t)(1-t^2)^{(p-3)/2}dt\,.$$

Spherical wavelet representation

The main idea of wavelet analysis is to obtain a multiscale representation of the data or functions which allows localization in space and frequency. The advantages of such splittings have been used recently in a variety of applications (cf. Freeden et al, 1998).

This idea will be exemplified for functions defined on $\Omega_3 \subset I\!R^3$, in particular for crystallographic pole functions; analogous results hold for orientation density functions defined on $\Omega_4 \subset I\!R^4$, and their one-to-one correspondence has recently been shown (Schaeben et al., 2001a). Generally, spherical wavelet analysis applies to any dimension p.

Initially, a pole density function is sampled on a coarse almost equidistributed grid on the sphere Ω_3. These measurements are approximated by a spherical polynomial of low degree. This polynomial is clearly a sufficiently good approximation in regions of the sphere where the underlying function does not oscillate too much or in other words consists of low frequencies, only. This approximation requires improvement in regions of the sphere where the initial data are largely oscillating. Therefore, additional measurements are required only locally. The crucial point is now the construction of a high degree polynomial from the globally coarse grid and the locally refine grid. This can be seen as adding adaptively and locally a wavelet part to the global approximation of low degree.

Any function F defined on Ω_3 may be associated with its harmonic series expansion

$$\begin{aligned} F(\mathbf{r}) &= \sum_{\ell=0}^{\infty}\sum_{n=-\ell}^{\ell} F_{\ell,n}Y_{\ell,n}(\mathbf{r}) \\ &= \sum_{\ell=0}^{\infty}\sum_{n=-\ell}^{\ell} < F(\circ), Y_{\ell,n}(\circ) > Y_{\ell,n}(\mathbf{r}) \qquad (1) \end{aligned}$$

with the inner product on the sphere with the surface element ds

$$< F_1, F_2 >= \int_{\Omega_3} F_1(\mathbf{r})\overline{F_2(\mathbf{r})}ds(\mathbf{r})\,.$$

The space of all spherical harmonics of degree ℓ with $\ell = 0, 1, 2, \ldots$, i.e. the restriction to the unit sphere of all homogeneous and harmonic polynomials in 3 variables, is denoted by $\mathcal{Y}_\ell$; then dim $\mathcal{Y}_\ell = 2\ell + 1$. The most important property of spherical harmonics here is their orthogonality relation. Namely, for $Y_{\ell,m} \in \mathcal{Y}_\ell$ and $Y_{k,n} \in \mathcal{Y}_k$ with $\ell \neq k$ it holds $< Y_{\ell,m}, Y_{k,n} >= 0$ and

$$\mathcal{L}^2(\Omega_3) = \overline{\bigoplus_{\ell=0}^{\infty} \mathcal{Y}_\ell}^{\mathcal{L}^2}\,,$$

i.e. any function in $\mathcal{L}^2(\Omega_3)$ may be represented by its harmonic series expansion.

Further, $\Pi_n(\Omega_3) = \bigoplus_{\ell=0}^{n} \mathcal{Y}_\ell$ with $\dim \Pi_n(\Omega_3) = (n+1)^2$.

Let $\{N_j\}$ be a sequence of strictly monotone increasing positive integers. Then scaling spaces V_j are introduced as polynomial spaces

$$V_j(\Omega_3) = \Pi_{N_j}(\Omega_3)$$

with dim $V_j(\Omega_3) = (N_j + 1)^2$. Hence there is a chain

$$V_0(\Omega_3) \subset V_1(\Omega_3) \subset V_2(\Omega_3) \subset \ldots$$

and it is sensible to define the corresponding orthogonal complements

$$W_j(\Omega_3) = V_{j+1}(\Omega_3) \ominus V_j(\Omega_3) = \bigoplus_{\ell=N_j+1}^{N_{j+1}} \mathcal{Y}_\ell$$

with $\dim W_j = (N_{j+1} - N_j)(N_{j+1} + N_j + 2)$. Finally,

$$\mathcal{L}^2(\Omega_3) = \overline{V_0(\Omega_3) \oplus \bigoplus_{j=0}^{\infty} W_j(\Omega_3)}^{\mathcal{L}^2}\,.$$

The classical approach of wavelet theory uses $N_j = 2^j$. However, in case of pole density functions defined on the unit sphere this would imply very large dimensions of the wavelet spaces. Therefore our choice in the calculations is more like $N_j = 20j$.

Using now

$$\sum_{k=-\ell}^{\ell} Y_{\ell,k}(\mathbf{r}_1)\overline{Y_{\ell,k}}(\mathbf{r}_2) = \frac{2\ell+1}{4\pi} P_\ell(\mathbf{r}_1 \cdot \mathbf{r}_2), \qquad \mathbf{r}_1, \mathbf{r}_2 \in \Omega_3$$

with Legendre polynomials P_ℓ of degree ℓ with $P_\ell(1) = 1$ results in

$$F(\mathbf{r}) = \sum_{\ell=0}^{\infty} < F(\circ), \frac{2\ell+1}{4\pi} P_\ell(\mathbf{r}\cdot\circ) >\,. \tag{2}$$

Considering harmonics only up to order N_j the approximation $S_{V_j}F(\mathbf{r})$ with respect to V_j is given by

$$S_{V_j}F(\mathbf{r}) = \sum_{\ell=0}^{N_j} < F(\circ), \frac{2\ell+1}{4\pi} P_\ell(\mathbf{r}\cdot\circ) > \tag{3}$$

and the corresponding next wavelet part by

$$S_{W_j}F(\mathbf{r}) = \sum_{N_j+1}^{N_{j+1}} < F(\circ), \frac{2\ell+1}{4\pi} P_\ell(\mathbf{r}\cdot\circ) > . \tag{4}$$

Introducing the kernel

$$G'_j(t) = \sum_{\ell=0}^{N_j} (2\ell+1) P_\ell(t)$$

it holds

$$S_{V_j}F(\mathbf{r}) = \frac{1}{4\pi} \int_{\Omega_3} F(\mathbf{r}') G'_j(\mathbf{r}\cdot\mathbf{r}') ds(\mathbf{r}') . \tag{5}$$

The right hand side can be numerically evaluated by a sampling theorem (cf. Potts et al, 1996), i.e.

$$S^I_{V_j}F(\mathbf{r}) = \sum_{\mathbf{k}\in I_j} w'_j(\mathbf{k}) F(\mathbf{r}'_{j,\mathbf{k}}) G'_j(\mathbf{r}\cdot\mathbf{r}'_{j,\mathbf{k}}) \tag{6}$$

with $I_j = \{\mathbf{k} = (k_1,k_2)^T \in I\!N_0^2 : k_1 < 2N_j, k_2 < 2N_j\}$ and

$$\mathbf{r}_{j,\mathbf{k}} = \left(\cos\frac{\pi k_1}{2N_j} \cos\frac{\pi k_2}{N_j}, \cos\frac{\pi k_1}{2N_j} \sin\frac{\pi k_2}{N_j}, \sin\frac{\pi k_2}{N_j} \right)^T$$

by using the Clenshaw–Curtis weights. Analogously, with

$$H'_j(t) = \sum_{\ell=N_j+1}^{N_{j+1}} (2\ell+1) P_\ell(t)$$

and

$$S^I_{W_j}F(\mathbf{r}) = \sum_{\mathbf{k}\in I_{j+1}} w'_{j+1}(\mathbf{k}) F(\mathbf{r}'_{j+1,\mathbf{k}}) H'_j(\mathbf{r}\cdot\mathbf{r}'_{j+1,\mathbf{k}}) \tag{7}$$

it holds

$$S^I_{V_{j+1}}F(\mathbf{r}) = S^I_{V_j}F(\mathbf{r}) + S^I_{W_j}F(\mathbf{r}) . \tag{8}$$

Substituting $S^I_{W_j}F(\mathbf{r})$ by

$$\hat{S}^I_{W_j}F(\mathbf{r}) = \sum_{\mathbf{k}\in I_{j+1}} w'_{j+1}(\mathbf{k}) L_j F(\mathbf{r}'_{j+1,\mathbf{k}}) H_j(\mathbf{r}\cdot\mathbf{r}'_{j+1,\mathbf{k}}) \tag{9}$$

with

$$L_j F(\mathbf{r}_{j+1,\mathbf{k}}) = \begin{cases} F(\mathbf{r}_{j+1,\mathbf{k}}) & \text{if } F \text{ is large,} \\ S^I_V F(\mathbf{r}_{j+1,\mathbf{k}}) & \text{otherwise,} \end{cases} \tag{10}$$

eventually yields

$$\hat{S}^I_{V_{j+1}} F(\mathbf{r}) = S^I_{V_j} F(\mathbf{r}) + \hat{S}^I_{W_j} F(\mathbf{r})\,. \tag{11}$$

Summarizing, the proposed procedure is as follows. The function $F(\mathbf{r})$ is known on a coarse $\mathbf{r}$–grid and $S^I_V f(x)$ is computed. By inspection or algorithms (cf. Mhaskar et al., 2001) the regions where $F(\mathbf{r})$ and $S^I_V F(\mathbf{r})$ have large absolute values and large oscillations, respectively, are detected. In the next step the approximation $S^I_V F$ is improved by adding the next wavelet part $S^I_W F$. Since $F(\mathbf{r})$ cannot be totally sampled on a refined $\mathbf{r}$–grid and since it is known that $S^I_W F$ is almost zero in regions where $F(\mathbf{r})$ does not oscillate too much, $S^I_V F + S^I_W F$ is replaced by $S^I_V F + \hat{S}^I_W F$. The definition of L_j shows that the function $F(\mathbf{r})$ must be resampled for some additional points in the regions where large oscillations of $F(\mathbf{r})$ are observed or expected (cf. Schaeben et al., 2001b).

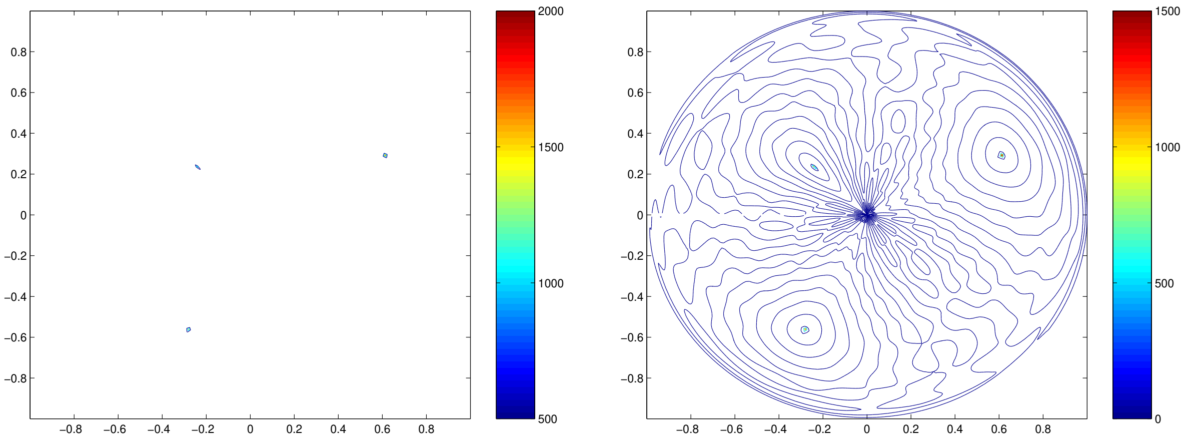

Figure 1: Given data on I_9 (left), error $S^I_{V_2} F(\mathbf{r}) - F(\mathbf{r})$ on I_9 (right).

In the following we give a numerical example. Figure 1 (left) shows the given data of a function $F(\mathbf{r})$ on a grid I_9. Figure 1 (right) shows the error $S^I_{V_2} F(\mathbf{r}) - F(\mathbf{r})$ on the full grid I_9. Note that

$$l_\infty = \max_{\mathbf{k}\in I_9} \left| S^I_{V_2} F(\mathbf{r}_{9,\mathbf{k}}) - F(\mathbf{r}_{9,\mathbf{k}}) \right| = 1951$$

and

$$l_2 = \sqrt{\sum_{\mathbf{k}\in I_9} \left| S^I_{V_2} F(\mathbf{r}_{9,\mathbf{k}}) - F(\mathbf{r}_{9,\mathbf{k}}) \right|^2} = 4298\,.$$

Figure 2 (left) shows the error using a much higher polynomial degree of 220. More precisely we show the error $|S^I_{V_{11}} F(\mathbf{r}) - F(\mathbf{r})|$ on the full grid I_9 and observe $l_\infty = 375$ and $l_2 = 1592$. Figure 2 (right) shows the error $\hat{S}^I_{V_2} F(\mathbf{r}) - F(\mathbf{r})$ which improve the results significantly, since $l_\infty = 28$ and $l_2 = 555$.

Finally we use only 25.3 % and 6.6 % of the given data and plot the errors $\hat{S}^I_{V_2} F(\mathbf{r}) - F(\mathbf{r})$ on I_9 in Figure 3 (left) and Figure 3 (right), respectively. Note that even if we use only 6.6 % of the given data the error $S^I_{V_{11}}(\hat{S}^I_{V_2} F(\mathbf{r})) - F(\mathbf{r})$ looks similar as in Figure 2 (left), where we used all data. In this case we obtain $l_\infty = 376$ and $l_2 = 1596$.

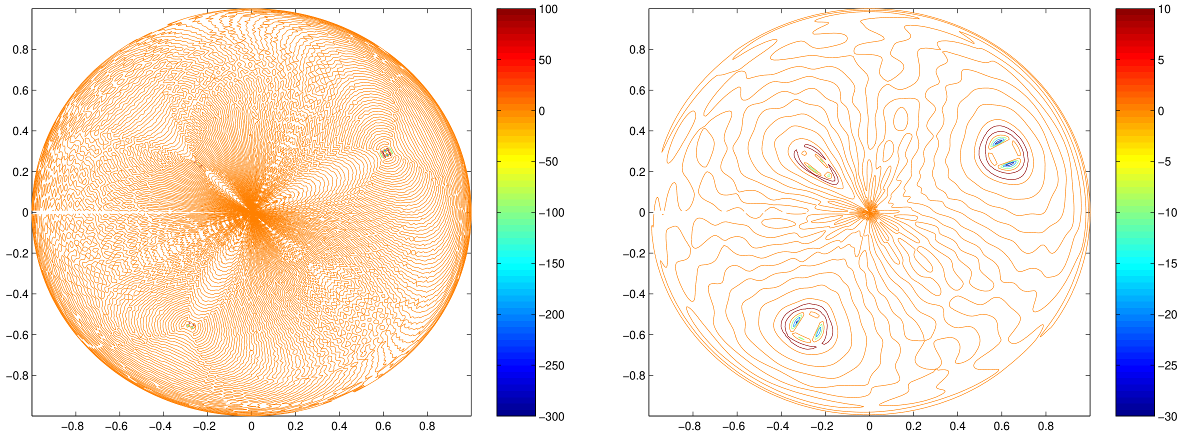

Figure 2: Error $S^I_{V_{11}}F(\mathbf{r}) - F(\mathbf{r})$ on I_9 (left), error $\hat{S}^I_{V_2}F(\mathbf{r}) - F(\mathbf{r})$ on I_9 (right).

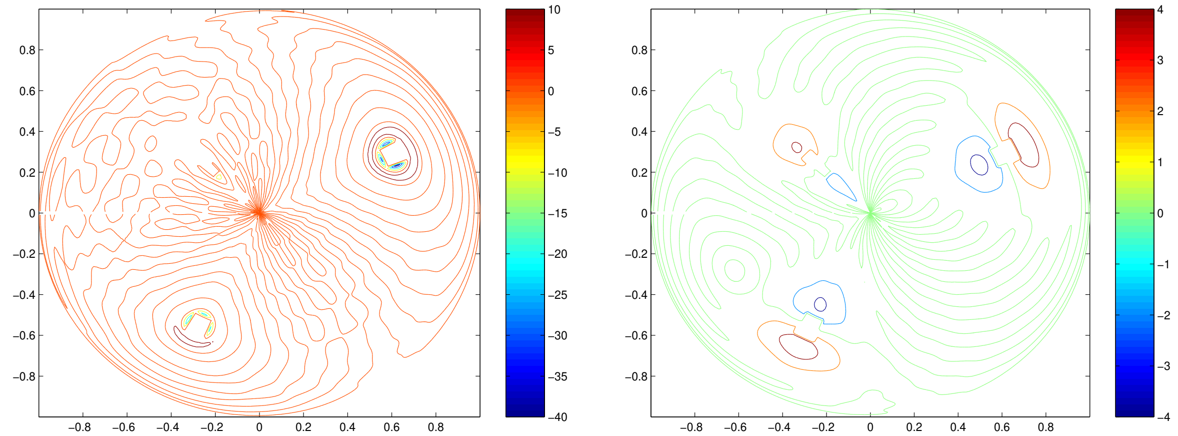

Figure 3: Error $\hat{S}^I_{V_2}F(\mathbf{r})-F(\mathbf{r})$ on I_9 using 25.3 % of the given data (left), error $\hat{S}^I_{V_2}F(\mathbf{r})-F(\mathbf{r})$ on I_9 using 6.6 % of the given data (right).

Spherical X–ray transform

A spherical X–ray transform of a function f defined on the sphere Ω_p is introduced as the mean of f along the circle spanned by two orthogonal elements $\mathbf{q}_1, \mathbf{q}_2 \in \Omega_p$. In particular, for $p = 4$, $\mathbf{q}_1, \mathbf{q}_2 \in \Omega_4$ can be interpreted as unit quaternions $q_1, q_2 \in I\!H$ representing (passive) rotations in $SO(3)$. In this special case the circle

$$C(q_1, q_2) = q_1 \cos t + q_2 \sin t = q(t), \quad t \in [0, 2\pi)$$

spanned by q_1, q_2 represents the set of all rotations mapping $\mathbf{r} := \mathrm{Vec}\,(q_1 q_2^{-1}) = \mathrm{Vec}\,(q_2 q_1^{-1}) \in \Omega_3$ on $\mathbf{h} := \mathrm{Vec}\,(q_1^{-1} q_2) = \mathrm{Vec}\,(q_2^{-1} q_1) \in \Omega_3$, i.e.

$$q^{-1}\mathbf{r}q = \mathbf{h} \ \text{ for all } q \in C(q_1, q_2)\,.$$

Therefore, the spherical X–ray transform $\frac{1}{2\pi}\int_{[0,2\pi)} f(q(t))dt$ of f for $p = 4$ may be thought of as a function defined on $\Omega_3 \times \Omega_3$ by

$$(Af)(\mathbf{h},\mathbf{r}) = \frac{1}{2\pi}\int_{C(q_1,q_2)} f(q)d\omega_2\,. \tag{12}$$

For more details the reader is referred to Schaeben et al., 2001c.

Since an even function f on Ω_4 is uniquely determined by its spherical Radon transform (cf. Schneider, 1969; Müller, 1998), it is also uniquely determined by its X–ray transforms Af (Nikolayev and Schaeben, 1999).

If f is a probability density function (of rotations), then its X–ray transforms Af are referred to as axes density functions in applied crystallography, and can be sampled as crystallographic pole density functions for given crystallographic axes $\mathbf{h}$ in a X–ray diffraction experiment.

For this case it has recently been shown (Schaeben et al., 2001a) that the spherical X–ray transform of the wavelet representation of f is the wavelet representation of the X–ray transform $Af(\mathbf{h},\circ)$, and that the wavelet representation can be applied to solve the inverse problem to determine numerically the crystallographic orientation density function f from experimental X–ray intensities measured in diffraction experiments with a texture goniometer.

Applications

Methods of high resolution texture analysis are required in crystallography to resolve the orientation distribution observed in very recent synchrotron radiation experiments (Wenk, 2001) of single crystals, which were conventionally thought of as being uniquely oriented.

High resolution texture analysis is also required in quality control of high tech materials where the ultimate goal is a perfect "single crystal" preferred orientation, as in high–temperature semi–conductors where the mean deviation from the "single crystal" peak orientation must not be larger than 1 degree. Similar problems arise in the analysis of "bamboo–structures" of single crystal wide copper wires on silicon wavers, or in thin epitaxial superconducting films, the electrical and magnetic properties of which are critical for their performance as electronic devices and need to be optimized.

Conclusions

The main idea of wavelet analysis is to obtain a multiscale representation of the data or functions which allows localization in space and frequency. In particular, the spherical wavelet representation of pole density functions corresponds to a hyperspherical wavelet representation of orientation density functions and vice versa. Thus, multiscale representation is transferred from one to the other and applies simultaneously.

The representation of sphercial functions, e.g. pole density functions, orientation density functions, spherical elevation models etc., by spherical wavelets

- is well suited to render them,

- provides a multiscale representation which allows for localization in frequency and space domain, i.e. adjusted to a locally refined grid according to large variations in the recorded data,
- provides means to design experimental devices with an automated adaptive control of the data sampling process adjusting the scan to a refined grid in areas of large data variations,
- applies in particular to the solution of the inverse texture problem due to the correspondence of the multiscale representation of pole and orientation density functions by virtue of (generalized) spherical wavelets.

References

[1] Freeden, W., Gervens, T., and Schreiner, M., 1998, Constructive Approximation on the Sphere with Applications to Geomathematics; Clarendon Press

[2] Hochstadt, H., 1986, The Functions of Mathematical Physics: Dover Publications

[3] Mhaskar, H. N., Narcowich, F.J., Prestin, J., and Ward, J.D., 2001, Polynomial frames on the sphere, to appear in: Advances in Computational Mathematics

[4] Müller, C., 1998, Analysis of Spherical Symmetries in Euclidean Spaces: Springer

[5] Nikolayev, D.I., and Schaeben, H., 1999, Characteristics of the ultrahyperbolic differential equation governing pole density functions: Inverse Problems 15, 1603-1619

[6] Potts, D., Steidl, G., and Tasche, M., 1996, Kernels of Spherical Harmonics and Spherical Frames, in Fontanella, F., Jetter, K., and Laurent, P.-J., (eds.), *Advanced Topics in Multivariate Approximation.* Singapore: World Scientific Publications, 287–301.

[7] Schaeben, H., Potts, D., and Prestin, J., 2001a, Wavelet representation of orientation and pole density functions: J. Appl. Cryst., submitted

[8] Schaeben, H., Prestin, J., and Potts, D., 2001b, Wavelet representation of diffraction pole figures: Advances in X–ray Analysis 44, in print.

[9] Schaeben, H., Sprößig, W., and Boogaart, K.G.v.d., 2001c, The Spherical X–ray Transform of Texture Goniometry: Proc. NATO Advanced Research Workshop on Clifford Anaylsis and Applications, Prague, Oct. 30 - Nov. 3, 2000, in print.

[10] Schneider, R., 1969, Functions on a sphere with vanishing integrals over certain subspheres: J. Math. Anal. Appl. 26, 381-384

[11] Wenk, H.R., 2001, oral communication